

16. Somewhat longer times apply in other low-order, mean-motion resonances. Similar results apply if the planet orbits inside the planetesimal.
17. If e_p is nonzero, there is a random walk in J , but this is much slower (by a factor of order e_p) than the random walk in E or L .
18. H. F. Levison and M. Duncan, *Icarus* **108**, 18 (1994). The lifetimes of Centaurs are similar [see L. Dones, H. F. Levison, M. Duncan, in *Completing the Inventory of the Solar System*, T. W. Rettig and J. M. Hahn, Eds. (Astronomical Society of the Pacific, San Francisco, CA, 1996), p. 233].
19. Equation 2 holds for planets the mass and size of Jupiter with orbital periods larger than about 50 days.
20. B. V. Chirikov, *Chaotic Dynamics in Hamiltonian Systems with Divided Phase Space* (Springer, Berlin, 1983); C. F. F. Karney, *Physica D* **8**, 360 (1983); N. Murray, *ibid.* **52**, 220 (1991).
21. H. F. Levison and M. Duncan, *Icarus* **127**, 13 (1997); M. J. Duncan and H. F. Levison, *Science* **276**, 1670 (1997).
22. By similar arguments, orbit-crossing planetesimals that collide with the star add energy to the planet; however, consumption by the star is much less common than ejection for planets at semimajor axes larger than a few stellar radii.
23. J. A. Fernández and W.-H. Ip, *Icarus* **58**, 109 (1984).
24. J.-C. Liou and R. Malhotra, *Science* **275**, 375 (1997).
25. The average radius $\alpha = (a/a_p) = (7/4)^{-2/3} = 0.7$ if the inner 7:4 resonance is the only relevant one.
26. E. J. Öpik, *Interplanetary Encounters* (Elsevier Scientific, Amsterdam, 1976).
27. A. Toomre, *Astrophys. J.* **139**, 1217 (1964); V. S. Safronov, *Ann. Astrophys.* **23**, 979 (1960); J. Binney and S. Tremaine, *Galactic Dynamics* (Princeton Univ. Press, Princeton, NJ, 1987).
28. M. Holman, J. Touma, S. Tremaine, *Nature* **386**, 254 (1997); K. A. Innanen, J. Q. Zheng, S. Mikkola, M. J. Valtonen *Astron. J.* **113**, 1915 (1997); T. Mazeh, Y. Krymowski, G. Rosenfeld, *Astrophys. J.* **477**, L103 (1997).
29. S. V. W. Beckwith, A. I. Sargent, R. S. Chini, R. Güsten, *Astron. J.* **99**, 924 (1990).
30. A possible concern with the interpretation of these observations is that the gas surface density may imply gravitational instability if the disk extends out to 100 AU. See the references in (27).
31. R. P. Butler, G. W. Marcy, E. Williams, H. Hauser, P. Shirts, *Astrophys. J.* **474**, L115 (1997); S. L. Baliunas, G. W. Henry, R. A. Donahue, F. C. Fekel, W. H. Soon, *ibid.*, p. L119; G. Gonzalez, *Mon. Not. R. Astron. Soc.* **285**, 403 (1997); G. Laughlin and F. C. Adams, <http://xxx.lanl.gov/abs/astro-ph/9710110>. "Planet swallowing" as a source of abundance anomalies in stellar atmospheres was first discussed by J. B. Alexander [*Observatory* **87**, 238 (1967)].
32. We acknowledge useful conversations with R. Malhotra and B. Paczyński. This research was supported by the Natural Sciences and Engineering Research Council of Canada and the Canadian Institute for Advanced Research.

26 August 1997; accepted 11 November 1997

Magnetic Properties of Hexagonal Closed-Packed Iron Deduced from Direct Observations in a Diamond Anvil Cell

Stuart Gilder* and Jonathan Glen†

The attraction of hexagonal closed packed (hcp) iron to a magnet at 16.9 gigapascals and 261 degrees centigrade suggests that hcp iron is either paramagnetic or ferromagnetic with susceptibilities from 0.15 to 0.001 and magnetizations from 1800 to 15 amperes per meter. If dominant in Earth's inner core, paramagnetic hcp iron could stabilize the geodynamo.

Fluid motion in Earth's liquid outer core generates a magnetic field that, when observed at the surface over several tens of thousands of years, resembles a dipole whose axis parallels Earth's rotational axis. However, the time-averaged field geometry may not depend on the fluid dynamics in the outer core alone. Recent numerical models suggest that a finitely conducting solid inner core stabilizes the geodynamo (1, 2). Deviations of the mean field from that of a geocentric dipole, such as the far-sided effect (3), could be explained if the inner core is composed of an aggregate of preferentially oriented hcp iron crystals (4). Such an aggregate could also explain why seismic waves traveling parallel to the rotational axis appear 1 to 4% faster than those traversing equatorial paths (5).

Although the phase of iron in the inner core is unknown, several studies conclude that the hcp (ϵ) phase is the best candidate

(6–8). Some work has suggested that convective flow in the inner core is sufficient to give ϵ -Fe a crystallographically preferred orientation (9, 10). Karato (11) proposed that the toroidal component of the field could give ϵ -Fe a preferred orientation such that its crystallographic c axis grows parallel to the rotation axis if the metal is paramagnetic with a certain degree of crystalline anisotropy of magnetic susceptibility (AMS) (12). The link between AMS in ϵ -Fe and field behavior was addressed by Clement and Stixrude (4), who assumed that magnetic susceptibilities of hcp metals other than Fe served as analogs for ϵ -Fe (9, 13). On the basis of this assumption, they assigned the magnetic susceptibility of ϵ -Fe to be 10^{-3} to 10^{-4} (SI units).

We used a nickel chromium alloy Merrill-Bassett diamond anvil cell (DAC). Iron (>99.9%) particles, generally spherical in shape with diameters of 1 to 5 μm , were loaded together with ruby chips and a pressure medium of methanol, ethanol, and water (16:3:1) into a ~ 100 - μm -diameter hole formed in a Re gasket. The cell was bolted to an insulating plate, which was in turn bolted to a motorized xy stage. A thermocouple was fixed in direct contact with the lower diamond. Three other thermocou-

ples surrounded the diamonds. An alternating current was applied to these thermocouples so that they functioned as resistive heaters. Pressure was measured several times during each experiment using the shift in the ruby R_1 peak (14) and temperature was measured continuously. Uniform melting of the pressure medium at low pressures suggests that no temperature gradient existed. The transparent pressure medium allowed the iron particles to be imaged with an optical microscope.

The DAC was heated in order to reduce the viscosity of the pressure medium so that the particles could move. A rare earth element magnet (measured magnetic moment $M_1 = 1.2 \text{ A}\cdot\text{m}^2$) was held 25 mm from the sample region with a pole pointed toward the cell, inclined $35^\circ \pm 10^\circ$ with respect to a horizontal plane. The magnet was held stationary or moved back and forth through an angle of $\sim 100^\circ$ about a horizontal plane to elicit a response from the particles. At a distance of 25 mm, fields measuring $1.2 \times 10^{-4} \text{ A/m}$ were induced in the sample region. The Inconel cell, stainless steel bolts, and Re gasket had negligible magnetizations. We assumed that the field of the magnet accounted for the total field in the sample region.

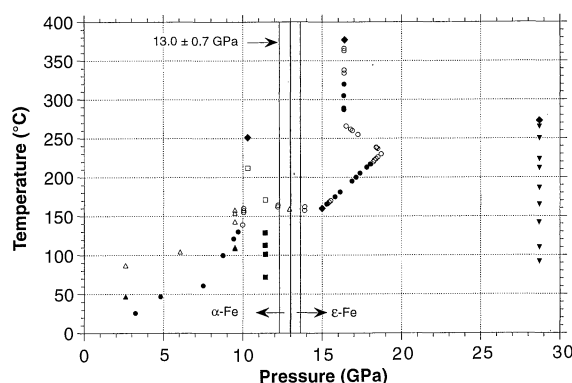
Particle motion was defined as either rotation or translation (Fig. 1). Motion of various particles was observed over a range of pressure and temperature during run 94.2.1 (Fig. 2). No motion was observed at 130°C and 9.7 GPa (Fig. 2A). At 140°C and 10.0 GPa, particle a migrated toward and collided with particle b (Fig. 2B). Between 155° to 160°C at 10.1 GPa, the combined particle ($a+b$) and particle c moved in response to the magnet. Particle $a+b$ migrated to the gasket wall at 165°C and 15.3 GPa (Fig. 2C). Between 166° to 366°C and 15.3 to 18.8 GPa, particles c and d (and others) responded to the magnet. Sometimes separate particles moved in concert with the motion of

S. Gilder, Institut de Physique du Globe de Paris, Laboratoire de Paléomagnétisme, 4 place Jussieu, 75252 Paris Cedex 05, France. E-mail: gilder@ipgp.jussieu.fr
J. Glen, Berkeley Geochronology Center, Berkeley, CA 94709, USA. E-mail: jglen@bgc.org

*Also at Institute of Tectonics, University of California, Santa Cruz, CA 95064, USA.

†Also at Earth Sciences Department, University of California, Santa Cruz, CA 95064, USA.

Fig. 1. Results from experiments 94.1.5 (squares), 94.1.6 (inverted triangles), 94.1.7 (triangles), and 94.2.1 (circles). Filled symbols = no particle motion; open symbols = particle motion; solid diamonds = cell failure.



the external field; at other times, no motion was observed, probably because the particles were pinned against a diamond wall. Lack of motion at low temperature (26°C) or high pressure (28.7 GPa) was likely due to a more viscous pressure medium. At 260°C and 16.9 GPa (Fig. 2D), particle *d* rotated in response to the applied field such that its long axis (12.5 μm in length) was perpendicular to the view direction. Particle *d* rotated again (2.5 μm by 2.5 μm in the view direction) at 261°C and 16.9 GPa when the magnet was removed (Fig. 2E). This particle is thus ellipsoidal with a volume *V* of $2.4 \times 10^{-16} \text{ m}^3$. When the magnet was returned to the cell, particle *d* moved toward it (Fig. 2, F through H), traversing a distance of 30 μm in 9.24 s (velocity $v = 3.2 \times 10^{-6} \text{ m/s}$) until it collided with particle *c* (Fig. 2I).

The motion of particle *d* about its minimum axis allows us to calculate the mean orientation of the maximum axis by measuring the apparent length of the ellipse several times during flight. We did so 38 times and found a mean apparent length of $6 \pm 2 \text{ μm}$, suggesting that the long axis was oriented $61^\circ \pm 10^\circ$ with respect to the horizontal.

The Fe particles were in the body centered cubic (bcc or α) phase when the experiments began. It is thus paramount to know the pressure and temperature at which Fe converts from the ferromagnetic bcc phase (15) to hcp. The boundary is hysteretic with near-vertical Clapeyron slopes of 455°, -283°, and -455°C per gigapascal and room-temperature transition pressures of 7.4, 13.5, and 9.0 GPa, respectively (7, 8, 16). The different pressure calibrations and pressure mediums used probably account for the inconsistencies. Von Bargen and Boehler (17) demonstrated that the width of the α - ϵ transition varies with increasing shear strength of the pressure medium. The mean transition pressure of all their experiments is $13.0 \pm 0.7 \text{ GPa}$. They postulate that crystal size is correlated to hysteresis width, with single crystals transforming to high-pressure phases faster than polycrystalline ones be-

cause the former have fewer grain boundaries and defects. In our experiments, the particles were small, the temperatures in the cell were above room temperature, and the pressure in the cell was hydrostatic. We therefore assumed that α -Fe completely converted to the ϵ phase at 13.0 GPa. Thus, the motion of the particles (Fig. 2, C to I) is interpreted as the response of ϵ -Fe.

The attraction of the particles to the magnet suggests they are either paramagnetic or ferromagnetic. Two possibilities must be considered for the former state: shape and crystalline AMS. If particle *d* responded to the magnet due to shape anisotropy, its long axis should be oriented parallel to the magnetic field during its flight. Because the pole piece was held $35^\circ \pm 10^\circ$ from the horizontal and the long axis was oriented $61^\circ \pm 10^\circ$, shape anisotropy can be ruled out. For the two remaining possibilities (ferromagnetic or crystalline AMS), we can quantify the moment magnetization M_2 for the former and bulk susceptibility χ for the latter.

The drag force F_d of the pressure medium acting against the particles can be represented by a Stokes resistance law of the form $F_d = 6\pi\mu vR$ (18), where μ is the fluid viscosity, v is the particle velocity, and R is a shape parameter. For a prolate ellipsoid with a maximum to minimum axis ratio of 5 that moves through a viscous fluid with no boundary conditions, $R = 5.93 \times 10^{-6} \text{ m}$. When wall effects are considered, the problem becomes more complex because the orientation of the ellipse changes with respect to the diamond walls, and the distance of the particle from the diamond surfaces is unknown. If the geometry resembles that in Fig. 2J, R will be about $9.0 \times 10^{-6} \text{ m}$. Viscosity of the pressure medium contributes the largest uncertainty. A power law extrapolation of the Stephan and Lucas (19) 252°C methanol data to 16.9 GPa gives an upper bound of $\mu = 1.2 \text{ mPa}\cdot\text{s}$. The viscosity of methanol at ambient conditions is $10^{-5} \text{ Pa}\cdot\text{s}$. If we take 1.2 mPa·s and $10^{-5} \text{ Pa}\cdot\text{s}$ as maximum and minimum estimates of μ with

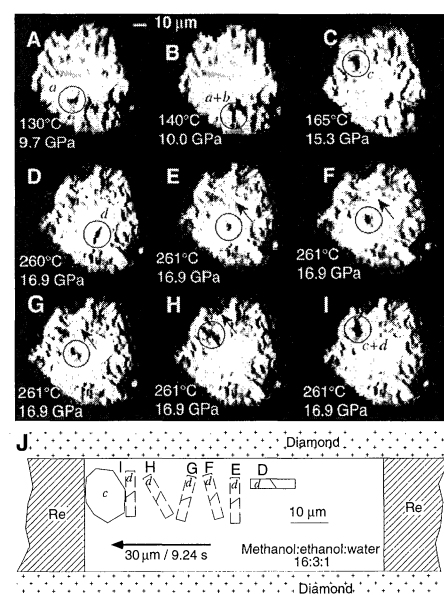


Fig. 2. (A through I) Images of the DAC during run 94.2.1. (J) Motion of particle *d* during frames (D) to (I).

$v = 3.2 \times 10^{-6} \text{ m/s}$, then $F_d = 6.5 \times 10^{-13}$ to $5.4 \times 10^{-15} \text{ kg}\cdot\text{m/s}^2$.

The force acting in the direction of motion F_r arises from the magnet-particle attraction. The particle moment M_2 equals JV for the ferromagnetic case and $\chi H_1 V$ for the paramagnetic case, where J is the magnetization and H_1 is the applied field. We find $F_r = M_2 \cdot \delta B / \delta r = JV \cdot \delta B / \delta r = \chi H_1 V \cdot \delta B / \delta r$ (20). Because $B = \mu_0 M_1 / 2\pi r^3$, $\delta B / \delta r = -3\mu_0 M_1 / 2\pi r^4$, and $H_1 = M_1 / 2\pi r^3 = B / \mu_0$, then $F_r = JV(-3\mu_0 M_1 / 2\pi r^4) \cos 35^\circ$ for the ferromagnetic case and $F_r = \chi V(-3\mu_0 M_1^2 / 4\pi^2 r^7) \cos 35^\circ$ for the paramagnetic case, where μ_0 is the permeability of free space ($4\pi \times 10^{-7} \text{ H/m}$) and r is the distance from M_1 to M_2 . Given the above values of M_1 , V , and r , the maximum and minimum values of χ and J are 0.15 to 0.001 and 1800 to 15 A/m, respectively.

Although our results cannot distinguish between the two magnetic states, we have constrained the values of χ and J . Previous studies on the magnetic properties of ϵ -Fe make it difficult to choose between the two. Using electron microscopy and shock wave techniques, Wasilewski (21) found that a magnetic phase change occurred when α -Fe transforms into antiferromagnetic ϵ -Fe. Although the samples were at room pressure during the analyses, his findings are consistent with extrapolations of Mössbauer effect and neutron diffraction studies that predict antiferromagnetic ordering of ϵ -Fe (22). More recent experiments using Mössbauer effect measurements did not detect ferromagnetic ordering of ϵ -Fe; however, only internal magnetizations above 0.05 T could be resolved (23). Band structure calculations

predict ϵ -Fe should not order magnetically (24), suggesting that it is paramagnetic.

The estimated values of χ offer constraints on existing models of Earth's magnetic field behavior, provided they remain valid at high core temperatures (4000° to 8000°C) and pressures (330 to 360 GPa). A paramagnetic inner core can explain a variety of geomagnetic phenomena (4), the source of which cannot be ascribed to processes acting in the outer core. The results of Hollerbach and Jones (1) and the recently developed three-dimensional dynamic models of Glatzmaier and Roberts (2) predict that a finitely conducting solid inner core would stabilize the geodynamo, because the inner core has a diffusive time scale independent of that of the outer core. We speculate the same could be true if the paramagnetic relaxation time of the inner core lags behind external field changes from the outer core. The outcome is that short-term fluctuations are damped out, and the dynamo is steadied. As a result, a brief breakdown of the dynamo would not lead to a successful reversal of the field. This inhibition to reversal, which results directly from the inner core's stabilizing influence on outer core convection, is feasible if our estimates are valid at core temperatures.

REFERENCES AND NOTES

1. K. Hollerbach and C. Jones, *Nature* **365**, 541 (1993).
2. G. Glatzmaier and P. Roberts, *ibid.* **377**, 203 (1995).
3. R. Merrill, M. McElhinny, D. Stevenson, *Phys. Earth Planet. Inter.* **20**, 75 (1979); X. Quidelleur, J. Valet, V. Courtillot, G. Hulot, *Geophys. Res. Lett.* **21**, 1639 (1994).
4. B. Clement and L. Stixrude, *Earth Planet. Sci. Lett.* **130**, 75 (1995).
5. A. Morelli, A. Dziewonski, J. Woodhouse, *Geophys. Res. Lett.* **13**, 1545 (1986); P. Shearer, K. Toy, J. Orcutt, *Nature* **333**, 228 (1988); X. Song and D. Helmberger, *Geophys. Res. Lett.* **20**, 2591 (1993).
6. O. Anderson, *Geophys. J. R. Astron. Soc.* **84**, 561 (1986); J. Brown and R. McQueen, *J. Geophys. Res.* **91**, 7485 (1986); H. Mao, P. Bell, C. Hadidiacos, in (7), pp. 135–138; Q. Williams, R. Jeanloz, J. Bass, B. Svendsen, T. J. Ahrens, *Science* **236**, 181 (1987); M. Ross, D. Young, R. Grover, *J. Geophys. Res.* **95**, 21713 (1990); C. S. Yoo, J. Akella, A. J. Campbell, H. K. Mao, R. J. Hemley, *Science* **270**, 1473 (1995).
7. S. Akimoto, T. Suzuki, T. Yagi, O. Shimomura, in *High-Pressure Research in Mineral Physics*, M. H. Manghnani and Y. Syono, Eds. (Geophysical Monograph 39, American Geophysical Union, Washington, DC, 1987), pp. 149–154.
8. M. H. Manghnani, L. Ming, N. Nakagiri, *ibid.*, pp. 155–163; R. Boehler, *Geophys. Res. Lett.* **13**, 1153 (1986).
9. H. Wenk, T. Takeshita, R. Jeanloz, G. Johnson, *Geophys. Res. Lett.* **15**, 76 (1988).
10. R. Jeanloz and H. Wenk, *ibid.*, p. 72.
11. S. Karato, *Science* **262**, 1708 (1993).
12. D. Farrell et al., *Phys. Rev. B* **36**, 4025 (1987); P. DeRango et al., *Nature* **349**, 770 (1991).
13. E. Collings and J. Ho, *Phys. Rev. B* **2**, 235 (1970); É. Volkenshtein, V. Galoshina, N. Shchegolikina, *Sov. Phys. JETP* **29**, 79 (1969); L. Stixrude and R. E. Cohen, *Science* **267**, 1972 (1995).
14. D. Adams, R. Appleby, S. Sharma, *J. Phys. E* **9**, 1140 (1976).
15. D. Collinson, *Methods in Rock Magnetism and Pa-*

- leomagnetism* (Chapman & Hall, New York, 1983).
16. E. Huang, W. Bassett, P. Tao, in (7), pp. 165–172; A. Jephcoat, H. Mao, P. Bell, *J. Geophys. Res.* **91**, 4677 (1986); W. Bassett and M. Weathers, *ibid.* **95**, 21709 (1990).
 17. N. Von Bargen and R. Boehler, *High Pressure Res.* **6**, 133 (1990).
 18. J. Happel and H. Brenner, *Low Reynolds Number Hydrodynamics* (Nijhoff, Boston, ed. 4, 1986).
 19. K. Stephan and K. Lucas, *Viscosity of Dense Fluids* (Plenum, New York, 1979).
 20. M. Rouault, *Électricité* (Masson, Paris, 1965).
 21. P. Wasilewski, *Adv. Earth Planet. Sci.* **1**, 123 (1977).
 22. H. Ohno, *J. Phys. Soc. Jpn.* **31**, 92 (1971); H. Ohno and M. Mekata, *ibid.*, p. 102; D. Pearson and J.

Williams, *J. Phys. F* **9**, 1797 (1979).

23. R. Taylor, G. Cort, J. Willis, *J. Appl. Phys.* **53**, 8199 (1982); G. Cort, R. Taylor, J. Willis, *ibid.*, p. 2064; R. Taylor, M. Pasternak, R. Jeanloz, *ibid.* **69**, 6126 (1991).
24. G. Fletcher and R. Addis, *J. Phys. F* **4**, 1951 (1974).
25. The generosity and guidance of E. Knittle and grants from the Earth Sciences Department, University of California, Santa Cruz, made this study possible. We thank S. Bigot, R. Coe, V. Courtillot, C. Jaupart, E. Knittle, M. LeGoff, J. Peyronneau, J. P. Poirier, and two anonymous reviewers for helpful discussions and comments. Institut de Physique du Globe de Paris contribution 1502.

14 August 1997; accepted 7 November 1997

Formation of Molecular Chlorine from the Photolysis of Ozone and Aqueous Sea-Salt Particles

K. W. Oum, M. J. Lakin, D. O. DeHaan,* T. Brauers,†
B. J. Finlayson-Pitts‡

Halogen atoms from the reactions of sea-salt particles may play a significant role in the marine boundary layer. Reactions of sodium chloride, the major component of sea-salt particles, with nitrogen oxides generate chlorine atom precursors. However, recent studies suggest there is an additional source of chlorine in the marine troposphere. This study shows that molecular chlorine is generated from the photolysis of ozone in the presence of sea-salt particles above their deliquescence point; this process may also occur in the ocean surface layer. Given the global distribution of ozone, this process may provide a global source of chlorine.

Sea-salt particles formed by wave action are ubiquitous in the marine boundary layer and in coastal regions. In addition, they have been found in some unusual situations such as in the plumes from the burning of the Kuwaiti oil wells (1). Chlorine atoms (Cl) formed from the reactions of sea-salt particles can destroy ozone (O₃), a key tropospheric oxidant (2–7) and greenhouse gas (8), through direct reaction. Alternatively, Cl reacts rapidly with organic molecules, which can, in turn, lead to O₃ formation in the presence of sufficient oxides of nitrogen (NO_x) (9).

Laboratory (2, 6, 7) and modeling (5, 10, 11) studies have shown that photochemically active, gas-phase Cl- and Br-containing compounds can be generated by a number of reactions of sea salt and its components. Although HNO₃ and H₂SO₄ displace HCl from sea-salt particles, this is not a significant source of atomic Cl because the subsequent reaction of HCl with

OH is relatively slow (12). Furthermore, the reactions of acids and oxides of nitrogen are insufficient under some circumstances to account for the measured Cl⁻ depletion (13), and a photochemical reaction of O₃ with aqueous sea-salt particles has been suggested as an alternative way of generating Cl₂. Although O₃ does not react at a significant rate with dry NaCl (14), laboratory studies have suggested that an unidentified photolyzable Cl-containing compound may form from sea-salt particles close to the deliquescence point in the presence of O₃ and probably light (15).

Field studies have identified photochemically active, gas-phase halogen compounds other than HCl in the troposphere (16–20), but specific compounds have been difficult to identify. Recently, Cl₂ was identified and measured in a coastal area (21) at concentrations up to 150 parts per trillion (ppt). This is a much larger concentration than can be attributed to known reactions of sea-salt particles, suggesting that there must be an unrecognized source producing a daily average of 280 ppt of Cl₂ per day.

We report the specific identification of Cl₂ as the product of the photolysis of O₃ in the presence of aqueous sea-salt particles in a controlled laboratory experiment. We used an aerosol chamber of 561 liters vol-

Department of Chemistry, University of California, Irvine, CA 92697–2025 USA.

*Present address: Department of Chemistry and Biology, Lyon College, Post Office Box 2317, 2300 Highland Road, Batesville, AR 72503–2317, USA.

†Present address: Institut für Atmosphärische Chemie, Forschungszentrum KFA, 52425 Jülich, Germany.

‡To whom correspondence should be addressed. E-mail: bjinlay@uci.edu